ChemPubSoc Europe

DOI: 10.1002/cctc.201902257

CHEMCATCHEM Full Papers

Polyol Synthesis of Ag/BN Nanohybrids and their Catalytic Stability in CO Oxidation Reaction

Anton S. Konopatsky,*[a] Denis V. Leybo,[a] Konstantin L. Firestein,[b] Ilya V. Chepkasov,[a, c] Zakhar I. Popov,[a, d] Elizaveta S. Permyakova,[a] Ilia N. Volkov,[a] Andrey M. Kovalskii,[a] Andrei T. Matveev,[a] Dmitry V. Shtansky,[a] and Dmitri V. Golberg[b, e]

Polyol method provides variety of options for microstructure control of a synthesized material. The present study aims to demonstrate that in case of Ag/*h*-BN nanohybrid fabrication the synthesis time requires precise tuning. Nonlinear correlation between synthesis time and Ag nanoparticles (AgNPs) formation and deposition is found and discussed. Catalytic stability of the studied system toward carbon monoxide oxidation is investigated for the first time. Two stages of catalytic activity decrease are found and associated with the sintering of AgNPs of the certain size. Correlations between Ag content, particle size distribution and temperature of complete CO conversion allow us to conclude that AgNPs, which size is below the critical value (3 nm), have a decisive role in Ag/BN nanohybrid catalytic performance. Density functional theory (DFT) calculations uncover the mechanism behind the increased catalytic activity of smaller AgNPs and highlight an importance of the Ag/BN interfacial regions.

Introduction

In many terms development of novel catalysts relies on success of materials science. During recent years novel nanostructured materials have attracted significant attention.[1,2] Among many advantages of novel nanostructures, high specific surface area is of the highest value. Indeed, availability of a great number of surfaces suitable for catalytically active nanoparticles (NPs) greatly benefits the material's functional properties. Appropriate combination of carriers and catalytically active elements leads to formation of prospective nanohybrid materials.[3–5] As for other attractive properties of the carriers for catalytically active NPs, one can outline high chemical stability and mechanical strength, as these materials are often supposed to work in an aggressive media. Hexagonal boron nitride (*h*-BN) demonstrates high resistance to oxidation and excellent mechanical properties.[6–8] For that reason *h*-BN attracts attention as prospective material for novel catalysts development.[9,10]

Various synthesis methods of BN-based catalysts have been implemented.[11–14] Chemical vapor deposition (CVD) provides sufficient control over content and homogeneity of catalytically active nanoparticles (such as Ag nanoparticles (AgNPs)) populating BN surfaces. On the other hand, decent performance the metal nanoparticles produced by that method is rather questionable.[15] Various chemical methods, such as wet impregnation method or polyol process, allow for precise control of the shape and size of metallic nanoparticles.[16–19] Many works have been dedicated to investigation of mechanisms and regularities of AgNPs formation *via* polyol process.[20,21] While concentration ratios of the polyol and $AgNO_3$ plays a significant role in reduction process and nanoparticles shape (as demonstrated for Ag nanocubes,)[22] introduction of additional components, such as NaOH and $NaBH_4$, opens new ways of control over the process. It has been demonstrated that NaOH significantly influences the reaction pathways and products composition, *i.e.* leads to formation of Ag_2O and $Ag(OH)_x$ species and accelerates the formation of AgNPs.[23] $NaBH_4$ has also been extensively used for reaction kinetics control, although hazardous environmental influence of this component impels the development of "green" synthesis schemes.[24]

Formation of colloid metal NPs and nanohybrid catalysts relies on similar methods, although additional complexity accompanied by the introduction of carriers may appear.[25] Interaction of catalytically active nanoparticles and their carriers plays a significant role in material's properties. In such manner it is suggested that in CO oxidation reaction active sites are on the contact perimeter between Au NPs and TiO_2 carriers, rather than on the surface of Au NPs.[26] Active sites stability during catalytic tests could be facilitated by the more intimate contact between catalyst components, as was demonstrated for the PdO-Co_3O_4 system.[27]

[a] Dr. A. S. Konopatsky, D. V. Leybo, Dr. I. V. Chepkasov, Dr. Z. I. Popov, E. S. Permyakova, I. N. Volkov, Dr. A. M. Kovalskii, Dr. A. T. Matveev, Prof. D. V. Shtansky
National University of Science and Technology "MISIS"
Moscow 119049 (Russia)
E-mail: konopatskiy@misis.ru
[b] Dr. K. L. Firestein, Prof. D. V. Golberg
Centre for Materials Science and School of Chemistry and Physics, Science and Engineering Faculty
Queensland University of Technology (QUT)
Brisbane QLD-4000 (Australia)
[c] Dr. I. V. Chepkasov
Katanov Khakas State University
Abakan 655017 (Russia)
[d] Dr. Z. I. Popov
Emanuel Institute of Biochemical Physics RAS
Moscow 119334 (Russia)
[e] Prof. D. V. Golberg
International Centre for Materials Nanoarchitectonics (MANA)
National Institute for Materials Science (NIMS)
Tsukuba 3050044 (Japan)

This manuscript is part of a Special Collection on the "French Conference on Catalysis".

Providing new material for a specific catalytic process requires complex characterization of its structure, as well as different catalytic tests. Catalytic activity of the material often plays the leading role in functional properties elucidation.[28–30] On the other hand, the results of catalytic stability tests demonstrate the specific material perspectives in different applications and also provide valuable fundamental data essential for better understanding of catalytic processes.[31,32]

In our study we focus on a simple approach toward Ag/BN nanohybrids synthesis *via* polyol method at room temperature implementing no additional components except BN nanoparticles (BNNPs), polyol and $AgNO_3$ solution. We extensively study Ag/BN nanohybrids catalytic performance. For the first time catalytic stability of the studied system is evaluated for CO oxidation reaction.

Results and Discussion

Structure of Ag/BN nanohybrids

Influence of the synthesis time on materials structure was evaluated using TEM method and the obtained results are given in Figure 1. As it follows from Figure 1a-h, the majority of AgNPs are in 1–10 nm range for all samples. AgNPs demonstrate crystalline structure, as confirmed *via* high-resolution transmission electron microscopy (HRTEM) imaging (Figure 1i–l). Interplanar spacings correspond well to Ag (111) 2.359 Å and *h*-BN (002) 3.333 Å values for all samples. As clearly follows from Figure 1a–d, the AgNPs size demonstrates a certain trend to change from very small (1–4 nm) to larger values as the synthesis time increases. Indeed, it could be suggested that at the shorter synthesis time $AgNO_3$ decomposition process is far from completion and small nanoparticles prevail. Once the number of individual AgNPs in the synthesis media is low, it could be suggested that the media (PEG) effectively stabilizes AgNPs and prevents their agglomeration and further growth. At the longer synthesis time (Figure 1b) the smaller AgNPs still dominate, but particles of larger sizes (in the range of 5–10 nm) can now be seen more frequently. A significant shift and qualitative change are observed for the Ag/BN_7 sample, as AgNPs mean size clearly shifts toward the larger values. The similar, but even more pronounced effect, is observed for the Ag/BN_20 and 60 samples (Figure 1g,h). It could be suggested that there is a specific correlation between Ag content and the particle size distribution. In order to verify this suggestion ICP analysis of all samples was conducted and the results are given in Table 1.

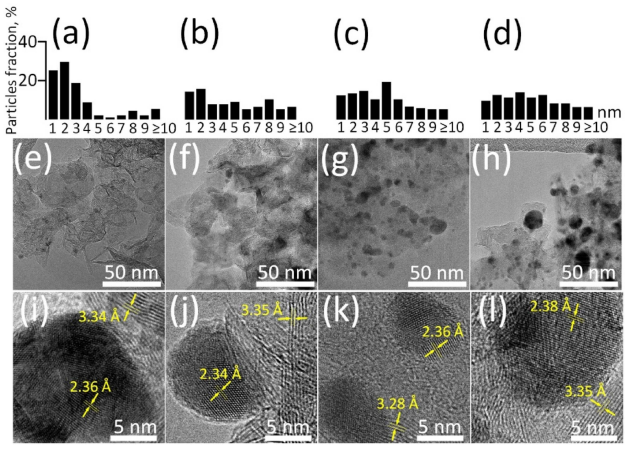

Figure 1. Ag/BN structure and AgNPs size distribution: (a), (e), (i) Ag/BN_2; (b), (f), (j) Ag/BN_7; (c), (g), (k) Ag/BN_20; (d), (h), (l) Ag/BN_60.

It can be seen from Table 1 that Ag content increases as the synthesis time prolongs. It is important to note that the change in Ag content is nonlinear. With increasing in synthesis time from 7 to 20 min, the Ag content increases almost 3 times and further does not notably change with time. This observation correlates well with AgNPs sizes distribution. Indeed, the most dramatic changes of the mean size are accompanied by the highest rate of Ag content increase. It means that the processes determining materials structure take place during the earliest synthesis stages. After some certain point (presumably after 20 min) almost no additional AgNPs are deposited over BNNPs surfaces and, mainly, the agglomeration of pre-formed AgNPs takes place which is reflected in size distribution changes (Figure 1d).

Chemical state of the obtained AgNPs was examined by XPS analysis (Figure 2). According to Figure 2, two peaks at approximately 368.4 and 374.4 eV are seen for all samples. Such binding energies indicate Ag3d 5/2 and Ag3d 3/2 signals, correspondingly. The gap of 6 eV between those peaks, as well as their asymmetric shape, especially apparent for Ag/BN_20 and Ag/BN_60 samples, point at the metallic state of Ag. XPS

Table 1. Results of ICP analysis.

Sample	Ag/BN_2	Ag/BN_7	Ag/BN_20	Ag/BN_60
Ag [wt.%]	0.96 ± 0.03	1.67 ± 0.02	4.65 ± 0.26	4.87 ± 0.13

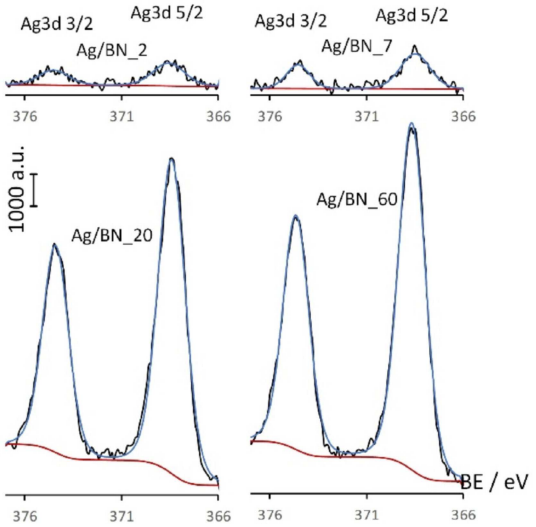

Figure 2. XPS spectra of AgNPs.

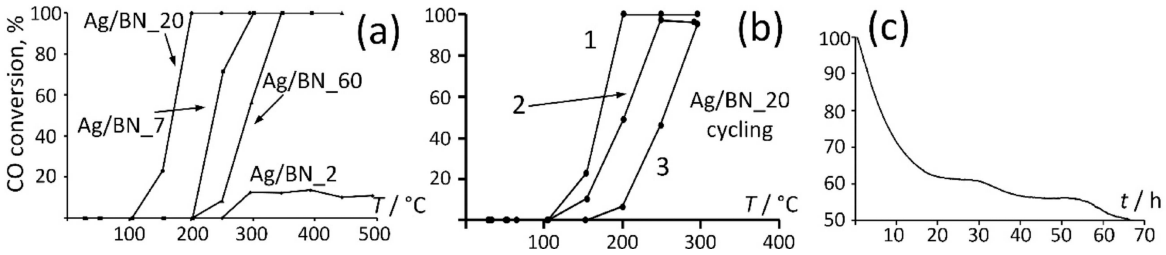

Figure 3. (a) Catalytic activity of all samples; (b) catalytic cycling and (c) catalytic stability of Ag/BN_20.

signal to noise ratio increases dramatically as we proceed from sample Ag/BN_7 to Ag/BN_20 and remains almost unchanged in case of Ag/BN_20 and Ag/BN_60, which is in good correspondence with ICP results (Table 1). It means that no significant changes in Ag chemical state occur as the synthesis time increases and the metallic state is preserved.

Catalytic performance

Results of catalytic performance tests are given in Figure 3. Figure 3a allows us to compare catalytic activity of all studied materials. Complete CO conversion is achieved for all samples except Ag/BN_2. The latter demonstrates only 18% of conversion at approximately 300 °C and further temperature increase doesn't lead to any improvement. Table 2 summarizes main factors related to the material's catalytic activity.

As follows from Table 2 the worst results are observed for Ag/BN_2 sample as it does not even reach full CO conversion and its offset temperature is the highest one. Ag/BN_60 sample, having the highest Ag content, demonstrates T_{100} of 345 °C, while Ag/BN_7 with 3 times lower Ag content has T_{100} of 300 °C. And the highest catalytic activity is observed for the Ag/BN_20 sample. A summary reflecting correlations between Ag content,

Table 2. Catalytic activity results.

Sample	Ag/BN_2	Ag/BN_7	Ag/BN_20	Ag/BN_60
CO conversion [%]	18	100	100	100
Conversion T [°C]	300	300	200	345
Offset T [°C]	250	200	100	200

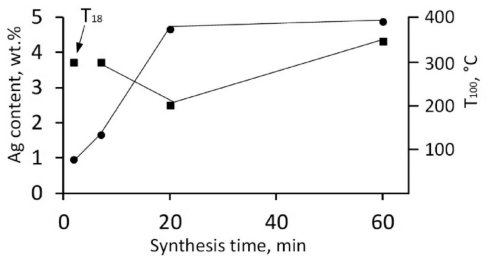

Figure 4. Correlation between Ag content, synthesis time and temperature of CO conversion. ■-T_{100}, (For Ag/BN_2 sample T_{18} is given); ●-Ag content.

CO conversion temperature and synthesis time is depicted in Figure 4.

In order to analyze Figure 4, a certain assumption should be discussed first. There are two main processes that should be taken into account while estimating influence of synthesis time on the materials structure, *i.e.* AgNPs formation and agglomeration rates. It is difficult to stabilize numerous individual AgNPs and their aggregation is more likely to occur. On the other hand, as the formation process of new AgNPs declines, the continuous agglomeration process is now dependent on already formed AgNPs, hence the whole process is hindered as well. In case of nanohybrids the formation rate of AgNPs is the highest during the first 20 min of synthesis, and the highest catalytic activity is peculiar to the Ag/BN_20 sample. From Figure 4 and Figure 1c, d it follows that there is some critical size of AgNPs and exceeding this size results in decreasing catalytic activity. On the other hand, it is also clear from Figure 4 and Figure 1b,c that a sufficient Ag content is mandatory for the enhanced catalytic activity of the material. Therefore, it can be suggested that for the studied system the most beneficial strategy (in terms of manufacturing more catalytically active materials) is to determine the period of the highest AgNPs formation rate and to select the optimal synthesis time within this period. It is also worth noting that in case of the studied materials catalytic activity solely depends on AgNPs morphology and content since, as it follows from Figure 2, their chemical states are identical.

Considering AgNP size distribution (Figure 1), Ag density (10.49 g/cc) and its content in each sample, the total and specific surface areas of AgNP are as follows: 6.7×10^{16} nm^2 and 138.5 m^2/g (Ag/BN_2), 9.2×10^{16} nm^2 and 110 m^2/g (Ag/BN_7), 24.7×10^{16} nm^2 and 106.4 m^2/g (Ag/BN_20), and 23.7×10^{16} nm^2 and 97.3 m^2/g (Ag/BN_60). The obtained results indicate that the highest AgNP total surface area is not a determining parameter providing the highest catalytic activity and, instead, the AgNP size effect should be taken into consideration. Reaction rates were calculated for the samples with full CO conversion according to the following Equation (1):

$$r\ (\mathrm{mmol\,g^{-1}s^{-1}}) = X_{co} \times Q \times C_f / w \qquad (1),$$

where Q is the total flow rate (mLs^{-1}), C_f is the initial CO concentration (mmol mL^{-1}), w is the Ag mass (g), and X_{co} is the conversion. For Ag/BN_7, Ag/BN_20, and AgBN_60 samples, the

following values were obtained: 1.6124, 0.5789, and 0.5528 mmol/g/s, respectively.

Different catalytic stability tests were performed for the Ag/BN_20 sample. These tests demonstrated its highest catalytic activity. As follows from Figure 3b, during the second run of catalytic cycling, nearly complete CO oxidation takes place (98% conversion) at a temperature of 250 °C, while at the third cycle 96% the conversion is reached at 300 °C. It implies the high reusability of the material toward CO oxidation reaction. Interestingly, the offset temperature rises only in case of the third run. The temperature interval, in which the reaction takes place, is quite narrow in case of the first cycle (100 °C) and increases up to 150 °C for other cycles. As for stability at the temperature of full CO conversion, it can be seen from Figure 3c that the material keeps a decent catalytic activity (more than 50%) even after 60 h of testing. Catalytic activity decrease could be explained considering two main stages. The first stage, during approximately first 18 h of testing, is characterized by the highest decrease in CO conversion (down to ~62%). During the following testing time (from 18 to 67 h) catalytic activity further decreases from 62 to 50%.

Table 3 compares the catalytic performance of different systems containing AgNPs.

It can be seen that from system to system temperature of complete CO conversion significantly varies. The highest catalytic activity is usually observed for oxygen-based substrates. For other substrate types, surface functionalization is required to provide enhanced catalytic activity.[38] Long-term catalytic stability is another important characteristic that is not only of great practical importance but also allows one to uncover deactivation mechanisms.

In order to determine the reasons behind catalytic activity decrease, the investigations of Ag/BN_20 sample structure and chemical state after catalytic stability test (designed as Ag/BN_20 stab) were conducted. The results of XPS and FTIR analyses are given in Figure 5.

It can be seen from Figure 5a that no additional components appear neither in Ag 3d 5/2 nor 3/2 and the gap between them remains at 6 eV, which indicates that Ag is still in its metallic state. The same conclusion follows from Figure 5b demonstrating that within the regarded region only the pronounced peaks (1366 and 783 cm^{-1}) of carrier's material (*h*-BN) are present.

As for materials microstructure, the noticeable changes can be observed. Figure 6 illustrates TEM images of Ag/BN_20 stab sample and AgNPs sizes distribution. As follows from Figure 6a a significant shift toward higher AgNP diameters is observed after catalytic stability tests. It is important that the shift affected smaller ($\leq$3 nm) AgNPs, which presumably have the highest impact on the materials catalytic activity. From Figure 6b it can be seen that while, in general, AgNPs density is still high, the number of the smallest AgNPs (1-3 nm) significantly decreases. It also follows from Figure 6 that sintering process of AgNPs takes place. It is especially vivid for the larger AgNPs (Figure 6b), but the traces of this process are also present for the smaller particles as well (Figure 6c). It can be suggested that the smaller AgNPs are more susceptible to sintering. The obtained results are in good correspondence with the catalytic activity tests. Indeed, the optimal equilibrium between AgNPs amount and their sizes facilitates the most pronounced catalytic effect, as it can be seen for the Ag/BN_20 sample (Figure 3a). The shift of this equilibrium toward the lower content (Figure 3a Ag/BN_7, Ag/BN_2) or larger sizes (Figure 3a Ag/bn 60) of AgNPs notably affects the catalytic performance. Catalytic cycling curves for the second and the

Table 3. Catalytic performance comparison.

Material	Ag [wt.%]	$T_{98\text{-}100}$ [°C]	T [°C]	t [h]	A [%]	Reference
Ag/BN	4.65	200	200	67	50	This work
Ag/Fe_2O_3	7	200	200	3.5	100	[33]
Ag/Co_3O_4	0.95	120	120	30	100	[34]
$Ag–Sn/CeO_2$	4	98	110	15	96	[35]
Ag/CeO_2	5	266	n/a	n/a	n/a	[36]
Ag/CeZr	4.5	350	n/a	n/a	n/a	[37]
Ag/FCNT	8.7	60	70	20	93	[38]
Ag/SiO_2	0.82	170	n/a	n/a	n/a	[39]

T – temperature of stability tests; t – total time of stability tests; A – catalytic activity after stability tests.

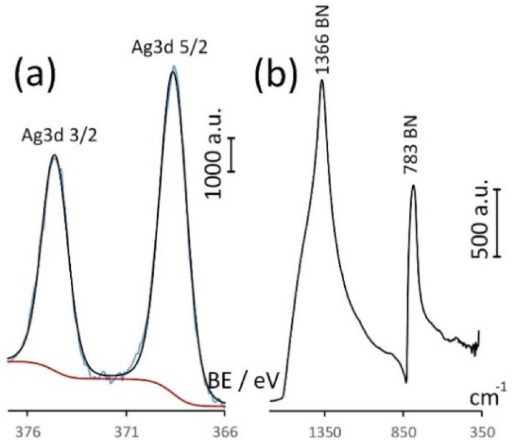

Figure 5. XPS (a) and FTIR (b) analysis Ag/BN_20 stab sample.

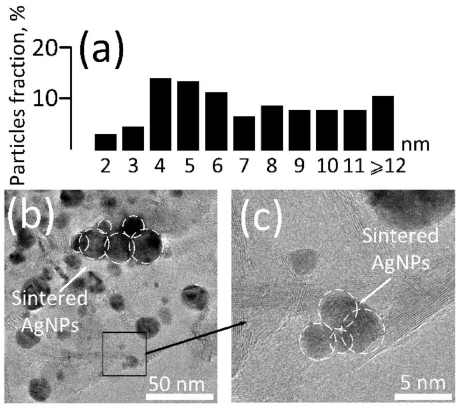

Figure 6. (a) AgNPs sizes distribution of Ag/BN_20 stab; (b), (c) Microstructure of Ag/BN_20 stab at different magnifications.

third runs resemble the results of catalytic activity tests for Ag/BN_7 and Ag/BN_60 samples. It can be suggested that the only difference is that in case of the second and third runs of Ag/BN_20 catalytic cycling the number of the most active AgNPs decreases as a result of their partial sintering during heating to 300 °C and in case of Ag/BN_2, Ag/BN_7 and Ag/BN_60 samples the number of the most effective AgNPs is not sufficient due to not optimal synthesis parameters. It means that the given particles (approximately in a range of 1–3 nm) have the highest influence on catalytic performance of the material.

The same approach holds for catalytic stability tests. It could also explain the appearance of two apparent stages of the catalytic activity decrease. One could suggest that the discussed sintering process would have a different pace at a given temperature for AgNPs with different sizes.

In such case, the sintering process of the smallest AgNPs would be significantly accelerated, as compared to larger particles. Taking into account their decisive role in materials catalytic performance it becomes clear that during the first stage of catalytic stability test (up to 18 h) the sintering of the smallest AgNPs takes place. More stable catalytic performance during the second stage supports the suggestion that the larger particles are more resistant to sintering at a given temperature.

Effect of NP size and distribution on catalytic activity

All three samples, namely Ag/BN_7, Ag/BN_20, and Ag/BN_60, demonstrate 100% of CO conversion. The reaction temperature interval is 100 °C for Ag/BN_7 and Ag/BN_20 samples and increases to 145 °C for Ag/BN_60 nanohybrid. Thus, the main advantage of Ag/BN_20 sample is that the offset and conversion temperatures are both 100 °C lower in comparison with Ag/BN_7 and Ag/BN_60 counterparts.

Size and surface density of catalytically active particles are the two main parameters affecting catalytic activity. The results indicate that the synthesis time significantly affects the Ag content by increasing the number of AgNPs and, to a lesser extent, their average size. After processing for 20 min, the surface of BN supports is heavily populated with AgNPs. With a further increase in processing time, the number of AgNPs does not increase and may even decrease due to NP agglomeration. However, the earlier formed NPs grow to larger sizes. As a result, the average AgNP size shifts to higher value (Figure 7). In case of Ag/BN_2, the Ag content and, accordingly, the number of AgNPs is too small to provide full CO conversion. Although the sample with 1.67 wt.% of Ag showed 100% of CO conversion, the AgNPs surface density was not high enough to initiate the reaction at a lower temperature. In case of Ag/BN_20 and Ag/BN_60 samples, which have quite similar Ag contents, the particle size becomes the dominant factor. Comparison of catalytic activities of these two samples clearly indicates that even a slight increase in NP size leads to a noticeable deterioration of catalytic performance in terms of offset and full conversion temperatures. Thus, it is reasonable to conclude that small size of catalytically active particles and their maximum density on the surface of BN supports are both required for enhanced catalytic performance. The size reduction of the catalytic nanoparticles gives rise to an increase in the number of under-coordinated atoms in the metal species. Correspondingly, the surface free energy of the metal subsystem increases, and the metal sites interact more strongly with the support and adsorbates, which accounts for the size effects of metal nanocatalysts. Finally, note that the size effect can become even stronger in the extreme case for single-atom catalysts when the size of individual catalytically active particle is decreased to a single atom and the density of doped atoms is high.[40]

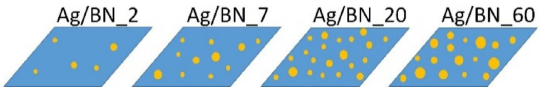

Figure 7. Schematic representation of AgNP size and distribution.

Calculation of the adsorption energy

NP size effect with respect to catalysis was addressed in several studies. It was suggested that small AgNPs have the ability to stabilize and activate oxygen species, hereby increasing catalytic activity.[41] The smaller the NP, the greater the likelihood that oxygen will be stabilized in the subsurface layer, which further enhances catalytic activity. On the other hand, the highest catalytic activity was reported for AgNPs in a size range of 3–5 nm.[39] This was explained by changes in electron-donating properties of AgNPs depending on their size.

We suggest that not only the size effect but also the substrate material can influence the catalytic activity of AgNPs. In order to verify this hypothesis, we have estimated the sorption energy of O_2 molecule to the Ag NP and the charge transfer to O_2 molecule assuming that the CO oxidation occurs by adsorbing O_2 molecule near the Ag/h-BN interface through the Eley-Rideal mechanism. The binding energy between O_2 and Ag/h-BN was calculated depending on the position of oxygen molecule, as shown in Figure 8. The results indicate that the presence of an oxygen molecule at the interface region (*i.e.* the lowest position in Figure 8) is the most energetically favourable (dE = −0.527 eV).

The Bader charge analysis shows the 1.18e transfer to oxygen molecule which fills the antibonding orbitals (see Figure 9).

When oxygen molecule is in other positions (Figure 8), the binding energy is lower ($dE = -0.049$ eV (middle position) and $dE = 0$ eV (upper position)) and the electron transfers are also low, 0.71e and 0.79e, respectively. The charge transfer correlates well with increasing the O–O distance in the oxygen molecule. These findings are consistent with the results of DFT calculations, indicating that the value of charge transfer from a pure Ag(110) surface to an O_2 molecule depends on its position.[42]

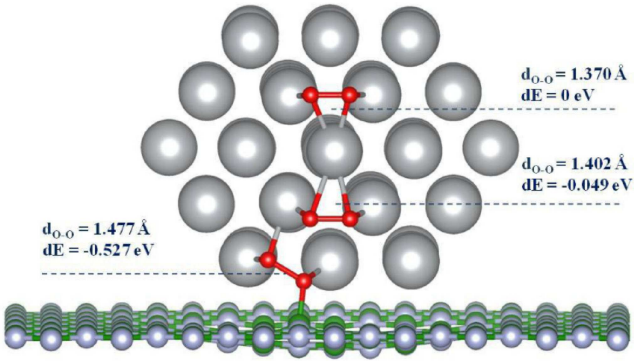

Figure 8. Oxygen molecule positions on AgNP/*h*-BN. The Ag, B, N, O atoms are marked as large grey, small green, small grey and red balls respectively.

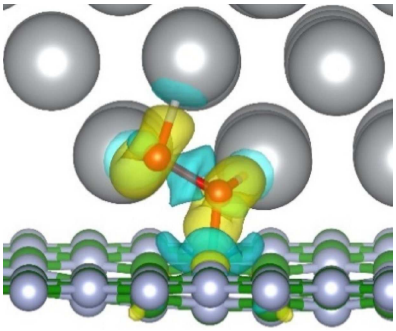

Figure 9. Charge difference between O_2 and AgNP/*h*-BN. The iso-surface level is equal to 0.005e/Å. The electron excess and deficiency regions are marked by yellow and cyan colours. The Ag, B, N, O atoms marked as big grey, small green, small grey and red balls, respectively.

The maximum value was approximately 0.9e, which is lower than in the case of the *h*-BN/AgNP interface.

High charge transfer suggests O_2-superoxide formation at the interface region.[43] In this case, CO can be directly oxidized to CO_2 by the superoxide without an energy barrier. This highlights the important role of the Ag/*h*-BN interface in the catalytic CO oxidation.

Conclusions

Ag/*h*-BN nanohybrids with Ag nanoparticles (AgNPs) 1–10 nm in size have been fabricated *via* a one-step polyol synthesis. During the synthesis, the Ag content increases rapidly in the first 20 min and further does not notably change with time, whereas the AgNPs size demonstrates a certain trend to change from very small (1-4 nm) to larger values. Once formed, metallic AgNPs do not change their chemical state. The catalytic activity toward CO oxidation increases in a row Ag/BN_2→Ag/BN_60→Ag/BN_7→Ag/BN_20. For the Ag/BN_20 sample, the onset temperature of catalytic CO oxidation is 100 °C and full conversion is completed at 200 °C. Ag/BN nanohybrids have high reusability toward CO oxidation reaction, as they withstand the consequent catalytic runs up to 300 °C with only insignificant decrease in CO conversion. The material keeps a decent catalytic activity (more than 50 %) even after 60 h of testing. Two stages of catalytic activity decrease are outlined: (i) rapid decrease in catalytic activity during the first 18 h due to sintering of the most active (~1–3 nm) AgNPs and slower decrease as a result of sintering of larger AgNPs. The enhanced catalytic performance of Ag/BN_20 sample is attributed to a small size of catalytically active AgNPs and their maximum density on the surface of BN supports. The important role of the Ag/h-BN interface in the catalytic CO oxidation is further supported by DFT calculations. It is demonstrated that the presence of an oxygen molecule at the interface region is the most energetically favorable. The high charge transfer suggests O_2-superoxide formation at the interface region. As a result, CO can be directly oxidized to CO_2 by the superoxide without an energy barrier.

Experimental Section

Curved BN nanosheets with an average size of 50 nm were used as carriers for Ag/BN nanohybrids synthesis. BNNPs preparatory annealing treatment is explained elsewhere.[44] 100 mg of BNNPs were dispersed in 50 ml of polyethylene glycol (PEG) (Mw = 400). 5 ml of 0.4 M $AgNO_3$ were added quickly to PEG with dispersed BNNPs at vigorous stirring at room temperature. The mixture of yellow colour during the first minutes of synthesis changed to dark brown at the maximum synthesis time. Different synthesis times, in a range from 2 to 60 min, were used to obtain the samples. Corresponding synthesis time in min is given in samples designation: Ag/BN_2, Ag/BN_7, Ag/BN_20, Ag/BN_60. The obtained samples were subjected to triple rinsing in distilled water in order to remove any secondary compounds. The samples were dried overnight without heating and used for catalytic tests.

Microstructure analysis was conducted using transmission electron microscopy (TEM) and high-resolution TEM (HRTEM) by means of a 200 kV JEM-2100 instrument. Chemical state of the materials surface was investigated by X-ray photoelectron spectroscopy (XPS) using an Axis Supra spectrometer (Kratos Analytical) and Fourier-transform infrared spectroscopy (FTIR) using a Vertex 70v (Bruker) instrument. The spectra were fitted using CasaXPS software, the Shirley-type background was used. Ag content was measured by inductively coupled plasma mass spectrometry (ICP-MS) using a iCAP Q device (Thermo Scientific). Synthesis media analysis was condcuted by UV-VIS spectroscopy (Ocean optics). For that an aliquote of the synthesis solution after centrifugation was collected and placed into a quartz cuvette for analysis.

Catalytic performance of the studied materials was analyzed toward carbon monoxide (CO) oxidation reaction. A sample (50 mg) diluted with quartz granules was placed in a fixed-bed continuous-flow reactor (U-tube) at ambient pressure. The activity measurements were conducted with 5.6 % CO, 11.2 % O2 and 83.2 % He gas flow under a total flow rate of 25 ml/min (GHSV = 43200 $ml \cdot gcat^{-1} \cdot h^{-1}$). Reaction products were analyzed by a mass-spectrometer (Thermostar). The conversion of CO gas was calculated using the Equation 2:

$$X = 1 - \frac{f^{f}_{CO}}{f^{i}_{CO}} \quad (2),$$

where f^{f}_{CO}-CO gas flow rate after the catalyst bed; f^{i}_{CO}-initial CO gas flow rate.

For catalytic cycling tests the sample was heated up to 300 °C, then cooled down to room temperature naturally and the cycle was repeated. In total three cycles were conducted. Catalytic stability tests were conducted at a temperature of the complete CO conversion obtained during catalytic activity tests. Duration of catalytic stability tests was 67 hrs.

All calculations were performed using VASP[45,46] in the framework of density functional theory (DFT) with Perdew, Burke and Ernzerhof (PBE)[47] exchange-correlation functional. The projector-augmented wave (PAW) based pseudopotentials were used to expand the plane waves basis sets with a cutoff energy of 400 eV. The DFT-D3 corrections[48] were used to take into account the Van der Waals interactions. Ag nanoparticle (55 atoms) with a diameter of 1.2 nm was located on *h*-BN monolayer consistisng of 120 atoms of N and 120 atoms of B. The Bader charge analysis[49] was performed for estimating the charge transfer between adsorbed oxygen and the *h*-BN/AgNP. As the close-packed (111) surface of silver has the lowest free energy[50] in our study the O_2 molecules were placed on the (111) surface of AgNP.

Acknowledgements

The authors gratefully acknowledge the financial support from the Ministry of Education and Science of the Russian Federation (Increase Competitiveness Program of NUST "MISiS" No. K2-2017-082, in the part of catalytic activity tests, and State Task No. 11.937.2017/ПЧ, in the part of Ag/BN characterization). D.G. is grateful for granting the Australian Laureate Fellowship No. FL160100089.

Conflict of Interest

The authors declare no conflict of interest.

Keywords: Ag/BN nanohybrids · polyol synthesis · CO oxidation · catalytic stability · microstructure characterization.

[1] K. S. Novoselov, D. Jiang, F. Schedin, T. J. Booth, V. V. Khotkevich, S. V. Morozov, A. K. Geim, The *Proceedings of the National Academy of Sciences* (PNAS) **2005**, *102*, 1–3.
[2] M. Naguib, V. N. Mochalin, M. W. Barsoum, Y. Gogotsi, *Adv. Mater.* **2014**, *26*, 992–1005.
[3] Q. Liu, J. Tian, W. Cui, P. Jiang, N. Cheng, A. M. Asiri, X. Sun, *Angew. Chem. Int. Ed.* **2014**, *53*, 6710–6714; *Angew. Chem.* **2014**, *126*, 6828–6832.
[4] J. L. Gunjakar, T. W. Kim, H. N. Kim, I. Y. Kim, S. J. Hwang, *J. Am. Chem. Soc.* **2011**, *133*, 14998–15007.
[5] X. Liu, J. Iocozzia, Y. Wang, X. Cui, Y. Chen, S. Zhao, Z. Li, Z. Lin, *Energy Environ. Sci.* **2017**, *10*, 402–434.
[6] D. Golberg, Y. Bando, Y. Huang, T. Terao, M. Mitome, C. C. Tang, *ACS Nano* **2010**, *4*, 2979–2993.
[7] A. Pakdel, Y. Bando, D. Golberg, *Chem. Soc. Rev.* **2014**, *43*, 934–959.
[8] D. V. Shtansky, K. L. Firestein, D. V. Golberg, *Nanoscale* **2018**, *10*, 17477–17493.
[9] C. Zhou, C. Lai, C. Zhang, G. Zeng, D. Huang, M. Cheng, L. Hu, W. Xiong, M. Chen, J. Wang, *Applied Catalysis B: Environmental* **2018**, *238*, 6–18.
[10] J. T. Grant, C. A. Carrero, F. Goeltl, J. Venegas, P. Mueller, S. P. Burt, S. E. Specht, W. P. McDermott, A. Chieregato, I. Hermans, *Science* **2016**, *354*, 1570–1573.
[11] B. Singh, P. Singh, K. Singh, J. Sharma, M. Kumar, R. Bala, R. Meena, S. K. Sharma, A. Kumar, *New Journal of Chemistry* **2017**, 11640–11646.
[12] Y. Ide, F. Liu, J. Zhang, N. Kawamoto, K. Komaguchi, Y. Bando, D. Golberg, *J. Mater. Chem. A* **2014**, *2*, 4150.
[13] F. F. Xu, Y. Bando, D. Golberg, M. Hasegawa, M. Mitome, *Acta Mater.* **2004**, *52*, 601–606.
[14] K. L. Firestein, D. G. Kvashnin, A. N. Sheveyko, I. V. Sukhorukova, A. M. Kovalskii, A. T. Matveev, O. I. Lebedev, P. B. Sorokin, D. Golberg, D. V. Shtansky, *Mater. Des.* **2016**, *98*, 167–173.
[15] K. L. Firestein, D. V. Leybo, A. E. Steinman, A. M. Kovalskii, A. T. Matveev, A. M. Manakhov, I. V. Sukhorukova, P. V. Slukin, N. K. Fursova, S. G. Ignatov, *Beilstein J. Nanotechnol.* **2018**, *9*, 250–261.
[16] H. Goto, A. Takagaki, R. Kikuchi, S. T. Oyama, *Appl. Catal. A* **2017**, *548*, 122–127.
[17] V. V. Dutov, G. V. Mamontov, V. I. Zaikovskii, L. F. Liotta, O. V. Vodyankina, *Appl. Catal. B* **2018**, *221*, 598–609.
[18] C. Ducamp-Sanguesa, R. Herrera-Urbina, M. Figlarz, *J. Solid State Chem.* **1992**, *100*, 272–280.
[19] Z. Jiang, M. A. Isaacs, Z. W. Huang, W. Shangguan, Y. Deng, A. F. Lee, *ChemCatChem* **2017**, *9*, 4268–4274.
[20] J. A. Adekoya, E. O. Dare, M. A. Mesubi, A. A. Nejo, H. C. Swart, N. Revaprasadu, *Results Phys.* **2014**, *4*, 12–19.
[21] Z. Yi, X. Xu, X. Tan, L. Liu, W. Zhang, Y. Yi, J. Luo, W. Yao, Y. Yi, T. Duan, *Surf. Coat. Technol.* **2017**, *327*, 118–125.
[22] B. Wiley, Y. Sun, B. Mayers, Y. Xia, *Chem. Eur. J.* **2005**, *11*, 454–463.
[23] S. Nishimura, D. Mott, A. Takagaki, S. Maenosono, K. Ebitani, *Phys. Chem. Chem. Phys.* **2011**, *13*, 9335.
[24] M. Blosi, S. Albonetti, S. Ortelli, A. L. Costa, L. Ortolani, M. Dondi, *New J. Chem.* **2014**, *38*, 1401–1409.
[25] F. Benedetti, P. Luches, M. C. Spadaro, G. Gasperi, S. Daddato, S. Valeri, F. Boscherini, *J. Phys. Chem. C* **2015**, *119*, 6024–6032.
[26] T. Fujitani, I. Nakamura, *Angew. Chem. Int. Ed.* **2011**, *50*, 10144–10147; *Angew. Chem.* **2011**, *123*, 10326–10329.
[27] Y. Sun, J. Liu, N. Yang, Y. Zhu, *ChemCatChem* **2017**, *9*, 738–745.
[28] T. Mazur, S. Lach, B. A. Grzybowski, *ACS Appl. Mater. Interfaces* **2017**, *9*, 44264–44269.
[29] N. Koukabi, E. Kolvari, M. A. Zolfigol, A. Khazaei, B. S. Shaghasemi, B. Fasahati, *Adv. Synth. Catal.* **2012**, *354*, 2001–2008.
[30] S. Özkar, *Appl. Surf. Sci.* **2009**, *256*, 1272–1277.
[31] G. Peng, C. Ludwig, F. Vogel, *ChemCatChem* **2016**, *8*, 139–141.
[32] L. Wang, F. S. Xiao, *ChemCatChem* **2014**, *6*, 3048–3052.
[33] A. Biabani-Ravandi, M. Rezaei, Z. Fattah, *Chem. Eng. J.* **2013**, *219*, 124–130.
[34] L. Li, Q. Yang, C. Zhang, J. Yan, Y. Peng, J. Li, *ACS Appl. Nano Mater.* **2019**, *2*, 3480–3489.
[35] I. A. Khan, N. Sajid, A. Badshah, M. H. S. Wattoo, D. H. Anjum, M. A. Nadeem, *J. Braz. Chem. Soc.* **2015**, *26*, 695–704.
[36] V. Abdelsayed, A. Aljarash, M. S. El-Shall, Z. A. Al Othman, A. H. Alghamdi, *Chem. Mater.* **2009**, *21*, 2825–2834.
[37] C. Lee, Y. Jeon, T. Kim, A. Tou, J. Il Park, H. Einaga, Y. G. Shul, *Fuel* **2018**, *212*, 395–404.
[38] Y. M. Dai, T. C. Pan, W. J. Liu, J. M. Jehng, *Appl. Catal. B* **2011**, *103*, 221–225.
[39] L. Yu, Y. Shi, Z. Zhao, H. Yin, Y. Wei, J. Liu, W. Kang, T. Jiang, A. Wang, *Catal. Commun.* **2011**, *12*, 616–620.
[40] X. Yang, A. Wang, B. Qiao, J. U. N. Li, *Acc. Chem. Res.* **2013**, *46*, DOI 10.1021/ar300361 m.
[41] M. Lamoth, M. Plodinec, L. Scharfenberg, S. Wrabetz, F. Girgsdies, T. Jones, F. Rosowski, R. Horn, R. Schlögl, E. Frei, *ACS Appl. Nano Mater.* **2019**, *2*, 2909–2920.
[42] T. B. Rawal, S. Hong, A. Pulkkinen, M. Alatalo, T. S. Rahman, *Phys. Rev. B* **2015**, *92*, 1–14.
[43] Y. Zhao, B. T. Teng, X. D. Wen, Y. Zhao, Q. P. Chen, L. H. Zhao, M. F. Luo, *J. Phys. Chem. C* **2012**, *116*, 15986–15991.

[44] A. Konopatsky, K. L. Firestein, D. V. Leybo, Z. I. Popov, K. Larionov, A. E. Steinman, A. M. Kovalskii, A. Matveev, A. Manakhov, P. B. Sorokin, *Catal. Sci. Technol.* **2018**, *8*, 1652–1662.
[45] G. Kresse, J. Furthmüller, *Phys. Rev. B* **1996**, *54*, 11169–11186.
[46] D. Joubert, *Phys. Rev. B* **1999**, *59*, 1758–1775.
[47] J. P. Perdew, K. Burke, M. Ernzerhof, *Phys. Rev. Lett.* **1996**, *77*, 3865–3868.
[48] S. Grimme, J. Antony, S. Ehrlich, H. Krieg, *J. Chem. Phys.* **2010**, *132*, DOI 10.1063/1.3382344.
[49] G. Henkelman, A. Arnaldsson, H. Jónsson, *Comput. Mater. Sci.* **2006**, *36*, 354–360.
[50] W. Luo, W. Hu, S. Xiao, *J. Phys. Chem. C* **2008**, *112*, 2359–2369.

Manuscript received: December 3, 2019
Revised manuscript received: December 30, 2019
Accepted manuscript online: January 9, 2020
Version of record online: February 3, 2020